

# Non-equilibrium Ionization and FIP Effect Diagnostics

Richard J. Edgar and Ruth Esser

Harvard-Smithsonian Center for Astrophysics, Cambridge, MA 02138

## ABSTRACT

We examine the accuracy of a common FIP effect diagnostic, the ratio of Ne VI to Mg VI lines in the solar transition region. Since the two ions have quite similar contribution functions near their maxima in equilibrium, the ratio of these two ions is often taken to be the abundance ratio of Ne and Mg. First we compute non-equilibrium ionization effects on the ratio  $f(\text{Ne}^{+5})/f(\text{Mg}^{+5})$  of ion fractions for a variety of simple flows through the transition region. Calculating the spectral line ratios for a few examples, we then show that non-equilibrium effects as well as temperature and density dependence must be evaluated for each line ratio used in the diagnostics.

*Subject headings:* Sun: corona – Sun: abundances – Sun: solar wind

## 1. Introduction

In many regions of the solar atmosphere (including the transition region, corona and solar wind) it appears that elements with a first ionization potential (FIP) greater than 10 eV are enhanced relative to those with  $\text{FIP} \lesssim 10$  eV. A common diagnostic to quantify this effect is the measurement of the ratios of emission lines of Mg VI (low FIP) and Ne VI (high FIP) (e.g. Jordan et al. (1998); Widing & Feldman (1989)). Both ions produce spectral lines in the neighborhood of 400 Å (minimizing possible calibration problems), and have very similar contribution functions in coronal equilibrium (see Fig. 1). This has been characterized as one of the best diagnostics for FIP-related abundances.

We calculate the ion fractions for both Ne and Mg ions, e.g.  $f(\text{Ne}^{+5}) \equiv n(\text{Ne}^{+5})/n(\text{Ne})$  (Fig. 1). We then compute the ion ratio  $F \equiv f(\text{Ne}^{+5})/f(\text{Mg}^{+5})$  in equilibrium (Fig. 2). There is a wide plateau near  $T = 4 \times 10^5$  K. It is this feature which is exploited when claiming this ion ratio should be insensitive to the details of the structure of the corona. The density ratio depends on the elemental abundances of Ne and Mg. The photospheric abundance of Ne is poorly known, and inferred from observations elsewhere in the solar system. However, the ratio of the total abundances of the two elements will alter our computed ratio everywhere only by a constant factor.

It can be seen in Fig. 2 that the ratio of the two ions at high temperatures is very different from that at temperatures where the maximum in the ion fraction curves occurs, even in the equilibrium situation. Before interpreting ratios of spectral lines formed by these ions as abundance ratios it is, therefore, necessary to establish that the plasma is predominantly at a temperature of  $\sim 4 \times 10^5$  K. To determine the distribution of ion fractions, needed to interpret the line ratio, one can observe a series of lines from multiple Ne and Mg ions (Young & Mason 1997).

In the present paper we presume that the elemental abundance ratio of Ne/Mg is fixed, and examine the effect of non-equilibrium ionization (NEI) situations. The code used to integrate the non-equilibrium ionization state of the gas is de-

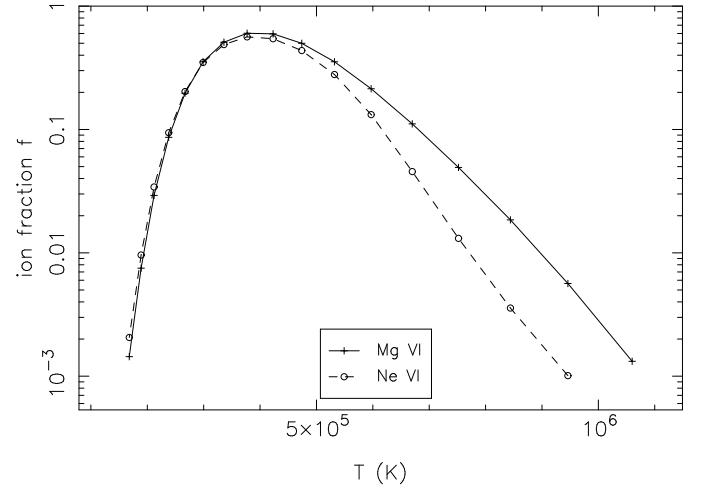


Fig. 1.— Ion fractions for Ne VI and Mg VI in coronal equilibrium.

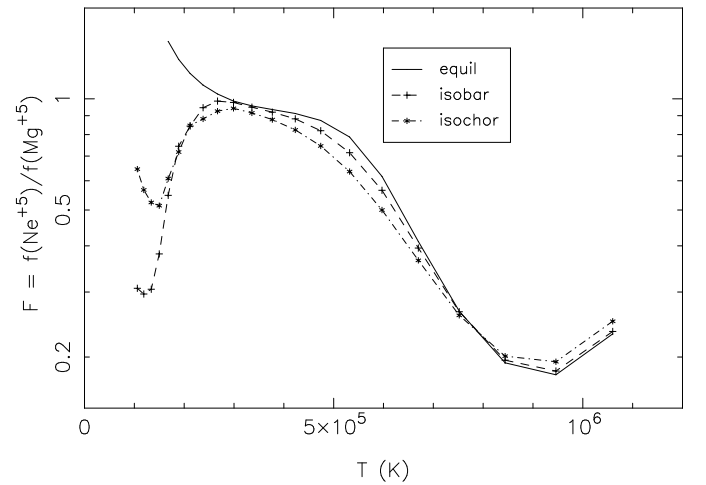


Fig. 2.— Ratio  $F$  of ion fractions for coronal equilibrium, and two cooling flow non-equilibrium ionization scenarios (constant pressure and constant density).

scribed elsewhere (Edgar and Chevalier 1986; Gaetz, Edgar and Chevalier 1988; Esser, Edgar and Brickhouse 1998). It uses

tabulated rate coefficients and cooling rates from Raymond & Smith (1977) as updated in 1993. We compute the rates in the low-density limit, which may affect the dielectronic recombination rates. The detailed shapes of the curves in Fig. 1 depend on what set of ionization and recombination rate coefficients are used, but the general conclusions presented here are independent of such choices.

The relevant comparison is between the time (or distance) scale over which the temperature changes significantly (such as the temperature scale height) and the ionization or recombination time (or distance) scale. The distance scales are given by

$$\lambda_{ion} = u/n_e C_{ion}, \text{ or } \lambda_{rec} = u/n_e \alpha_{rec}, \quad (1)$$

where  $n_e$  is the electron density,  $u$  is the flow speed,  $C_{ion}$  and  $\alpha_{rec}$  are ionization and recombination rate coefficients in units of  $\text{cm}^3 \text{s}^{-1}$ , respectively (Maxwellian averaged  $\langle \sigma v \rangle$ , where  $\sigma$  is the cross section and  $v$  is the random relative speed of electrons and ions).

## 2. Non-Equilibrium Flows

### 2.1. Recombining

As an example of a recombining flow, we look at the situation described by Edgar and Chevalier (1986), namely a hot gas ( $T_h \sim 10^6 \text{ K}$ ) permitted to cool (and recombine) due only to its own radiation. For  $T \lesssim 10^6 \text{ K}$ , the gas cools faster than it recombines, producing an over-ionized situation. This is similar to a microflare condition.

We have computed two cases, and the results are plotted in Fig. 2. The two situations are cooling at constant pressure (isobarically), and at constant density (isochorically). Note that for  $T \gtrsim 2.5 \times 10^5 \text{ K}$ , while the details differ a bit, the ion ratio  $F$  is quite similar to that in equilibrium. However, at lower temperatures, the departure from equilibrium is quite extreme, reaching perhaps an order of magnitude in the isobaric case.

The time scale for temperature change is given by the cooling time,  $t_{cool} = T/(dT/dt)$ . Since both the recombination and cooling rates vary directly with density, “fluence” ( $\int n_e dt$ , units  $\text{cm}^{-3} \text{s}$ ), is the natural independent variable instead of time. (For example, for density  $10^9 \text{ cm}^{-3}$ , a fluence of  $10^{10} \text{ cm}^{-3} \text{s}$  is reached in 10 s.) If the recombination time  $1/n_e \alpha_{rec}$  becomes longer than the cooling time, or equivalently the recombination coefficient becomes less than the inverse cooling fluence,  $\alpha_{rec} \lesssim 1/n_e t_{cool}$ , recombination will lag behind the temperature change. This effect can be seen in Fig. 2 for  $T \lesssim 2.5 \times 10^5 \text{ K}$ .

As a more extreme case of a recombining plasma, we consider a gas taken to be at coronal equilibrium at an initial high temperature  $T_h \sim 10^6 \text{ K}$ , instantaneously reset to a cold temperature, of  $10^4 \text{ K}$ . We then follow the recombination of Ne and Mg through the various ionization states, as functions of the fluence  $\int n_e dt$ . We plot  $F$  in Fig. 3, and the ionization fractions of  $\text{Ne}^{+5}$  and  $\text{Mg}^{+5}$  in Fig. 5 (downflow case). Note that in the recombining case, the curves for the two ions are very different, which leads to a change in  $F$  by an order of magnitude during the recombination. This is caused by the fact that the Ne recombines through the +5 state sooner than the Mg does. This example might represent an extreme case of downflow through the transition region.

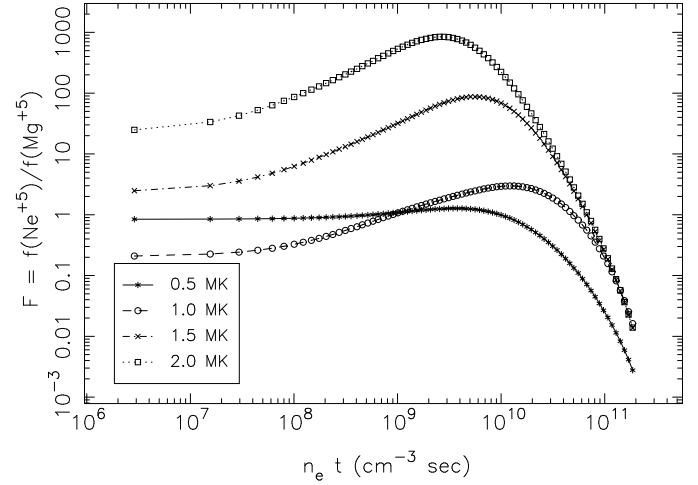


Fig. 3.— Ratio  $F$  of ion fractions vs. fluence ( $\int n_e dt$ ) for four sudden cooling models. Initial high temperatures  $T_h$  are given in MK.

It is of course true that the details of this calculation depend on the initial conditions, in particular on the ionization states of Ne and Mg in the gas. Real flows in the solar corona will be more complex, and one must have an idea of the history of the gas before it begins the downward flow through transition region temperatures in order to know what initial conditions are appropriate. However, the large variability of  $F$  in this example shows that downflows must be treated with caution, when interpreting  $F$  as an abundance ratio. (See also section 2.3.)

### 2.2. Ionizing

An extreme example of an ionizing plasma is a shock, which instantaneously changes the temperature from  $10^4 \text{ K}$  to of order  $10^6 \text{ K}$ . The results are independent of the initial temperature as long as it is low compared to the temperature range at which the ions form (e.g.  $< 10^5 \text{ K}$ , see Fig. 1). In the ensuing flow, we watch as Ne and Mg atoms ionize up beyond the +5 state, and compute the ion ratio.

The ratio  $F$  is shown as a function of fluence for four different shock scenarios with “post-shock” temperatures  $T_h$  of 0.5, 1.0, 1.5, and  $2.0 \times 10^6 \text{ K}$  in Fig. 4. The gas is then followed towards the new equilibrium situation. For  $T_h = 2 \times 10^6 \text{ K}$ , the ratio  $F$  varies by about one order of magnitude, but it is relatively constant and of order unity for  $T_h = 1.0 \times 10^6 \text{ K}$ . Ion fractions  $f$  are shown for this case in 5.

Upflows through the transition region, modeled in the following section, are similar to this situation.

### 2.3. Solar Wind Flows and Downflows

The characteristics of the solar wind flow in the critical region, from the top of the transition region at about  $10^5 \text{ K}$  to the corona at about  $10^6 \text{ K}$ , are not well known. As an example we have chosen the electron density, temperature and proton flow speed from a model by Hansteen, Leer, and Holzer (1997) (Fig. 6), as this model is the only one to date that calculates the onset of the solar wind from the mid-chromosphere to the corona self consistently. In the calculations of the ion fractions shown in Figure 7, we have assumed that the Ne and Mg ions flow with

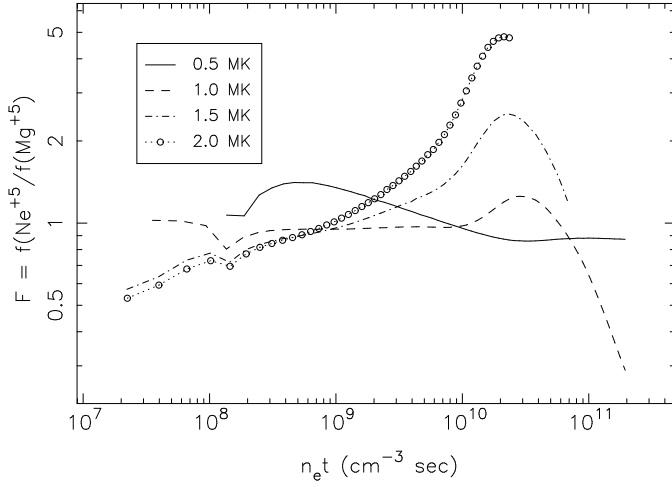


Fig. 4.— The ratio  $F = f(\text{Ne}^{+5})/f(\text{Mg}^{+5})$  ion fractions vs. fluence ( $\int n_e dt$ ) for four shock models. Post-shock temperatures are given in MK.

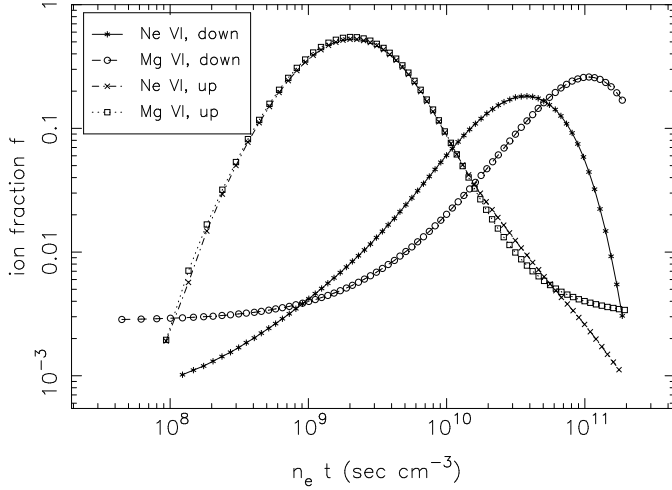


Fig. 5.— Non-equilibrium ion fractions vs. fluence, for the case of  $T_h = 10^6$  K, for both ionizing (upflow) and recombining (downflow) models.

the same speed as the protons. Note that this non-equilibrium case shows a much wider region in temperature space where  $F$  is of order unity. Essentially the same curve is obtained if we arbitrarily multiply the flow speed by 10. The equilibrium case (Fig. 2, solid line) is shown as a comparison.

This scenario is somewhat similar to the shock flows presented above (Sec 2.2), since the flow is fast enough that the temperature changes significantly in less than an ionization time:

$$t_{ion} = \frac{1}{n_e C_{ion}} \gtrsim \frac{1}{u} \frac{T}{|\nabla T|}. \quad (2)$$

This similarity is perhaps not surprising as the transition region is quite steep, and ends at a temperature of the order of  $10^6$  K, as in one of the shock models (dashed line in Fig. 4).

Downflows are common in the transition region. However, the details such as velocity or temperature profile vs. height are often elusive. Here we take as an example a time-reversed version of the upflow model above. The ionization state of the gas at the beginning of the downflow is needed for the model, but depends on the prior history of the gas. We presume the gas is in coronal equilibrium at two temperatures, 0.6 and  $0.8 \times$

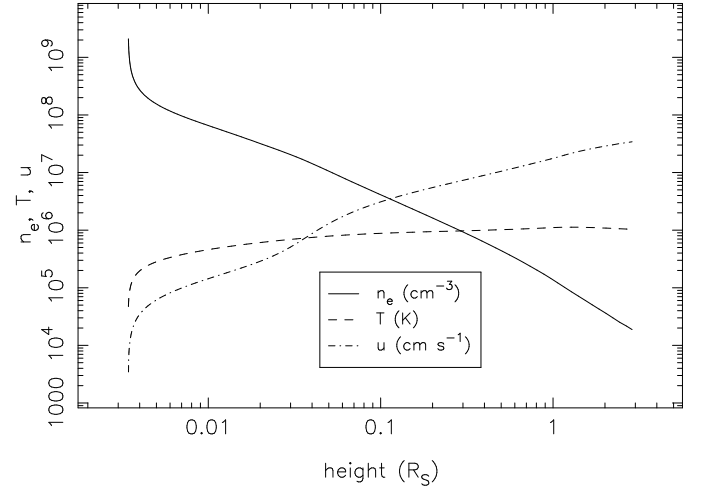


Fig. 6.— Density, temperature and velocity vs. height for the flow model of Hansteen, Leer, and Holzer (1997).

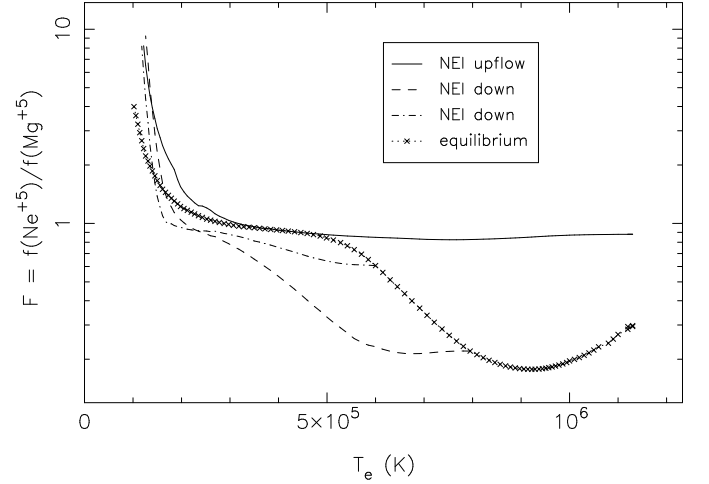


Fig. 7.— The ratio  $F = f(\text{Ne}^{+5})/f(\text{Mg}^{+5})$  ion fractions for the upflow model of Hansteen, Leer, and Holzer (1997), and for the analogous time-reversed downflow model.

$10^6$  K. The resulting ion ratios  $F$  are plotted in Fig. 7. They start (on the right of the figure) at the equilibrium curve (the assumed initial condition), and move to the left toward lower temperatures with time. Starting from  $0.8 \times 10^6$  K, the ion ratio starts at low values and comes up to nearly unity. The details are somewhat different from the sudden cooling model discussed above (Sec. 2) due to the fact that the flow decelerates towards lower temperatures as the density rises rapidly. This causes the ionization state to approach coronal equilibrium at the end of the flow. Nonetheless, we see that this downflow also has an ion ratio  $F$  significantly different from unity over the part of the flow where the ions are abundant.

## 2.4. Emissivity Calculations

In this section we discuss the intensity ratios of the spectral lines most commonly used for abundance ratio determination for these two ions. The Ne VI lines are transitions from  $2s2p^2 \ ^2P_{3/2} \rightarrow 2s^22p^2 \ ^2P_{3/2,1/2}$  ( $\lambda\lambda 401.93, 399.82$ ), and  $2s2p^2 \ ^2P_{1/2} \rightarrow 2s^22p^2 \ ^2P_{3/2,1/2}$  ( $\lambda\lambda 403.26, 401.14$ ), while the Mg VI lines connect  $2s2p^4 \ ^4P_{1/2,3/2,5/2} \rightarrow 2s^22p^3 \ ^4S_{3/2}$

( $\lambda\lambda 399.28, 400.66, 403.31$ ). Emissivity calculations were performed using the APEC code (Smith & Brickhouse 2000), with atomic data taken from the CHIANTI database (Landi et al. 1999). Energy levels for both Ne VI and Mg VI are taken from Martin et al. (1995). Collision and oscillator strengths for Ne VI are from Zhang et al. (1994) and Dankwort & Treffitz (1978), respectively. Those for Mg VI are taken from Bhatia & Mason (1980).

The interpretation of emissivity ratios is even more complicated, as the emissivities of these lines, and their ratios, depend on both density and temperature. As examples, we plot in Fig. 8, the ratio Ne VI  $\lambda 401.14$ /Mg VI  $\lambda 399.28$  for three of the above models: equilibrium ionization, isobaric cooling (with pressure  $n_e T = 2.6 \times 10^{14} \text{ cm}^{-3} \text{ K}$ ), and the Hansteen, Leer, and Holzer (1997) upflow model. To demonstrate the density dependence, the equilibrium curve is shown for two densities,  $10^7$  and  $10^{11} \text{ cm}^{-3}$ . Note that the region of weak temperature dependence ( $T \approx 2 - 5 \times 10^5 \text{ K}$ ; e.g. Fig. 2) has more or less disappeared.

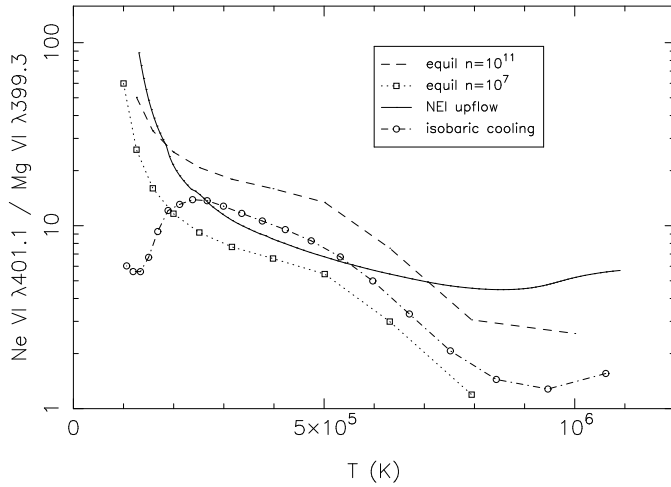


Fig. 8.— The ratio Ne VI  $\lambda 401.1$ /Mg VI  $\lambda 399.3$  of line emissivities for coronal equilibrium at two densities, for the isobaric cooling case, and for the upflow model of Hansteen, Leer, and Holzer (1997).

These examples demonstrate that non-equilibrium effects as well as temperature and density dependence must be evaluated for each line ratio used in the diagnostic.

### 3. Summary and Discussion

The Ne<sup>+5</sup> to Mg<sup>+5</sup> line ratio diagnostic is generally based on the assumption that the ions are in ionization equilibrium and that the plasma is predominantly at temperatures between  $2$  and  $5 \times 10^5 \text{ K}$ . Below and above that range, temperature effects are important (e.g. Fig. 2). The goal of the present paper was to investigate the effects of non-equilibrium situations on  $F \equiv f(\text{Ne}^{+5})/f(\text{Mg}^{+5})$ . If the plasma is not in equilibrium, assumptions regarding the plasma dynamics and prior history have to be made, since plasma parameters describing these flow dynamics are often unknown.

To shed some light on NEI effects we have considered a number of idealized cases. Some of these cases, isobaric and isochoric cooling (Fig. 2) and ionizing shock situations (Fig. 4) maintain an ionization balance for the two ions extremely

close to the equilibrium values. In the presence of outflow, as in a solar wind situation where the flow speed in the transition region is small  $\lesssim 10 \text{ km s}^{-1}$ , the ratio of the two ions actually remains close to 1 over a larger temperature range (Fig. 7, solid line). However, calculating the spectral line ratios for a few examples shows that this effect vanishes due to the presence of a density dependence (Fig. 8) which exists for both equilibrium and NEI conditions.

In situations resembling downflows, on the other hand, in which the plasma cools quickly (Figs. 3 and 7, dash and dash dotted lines), the deviation from equilibrium might be quite significant. The two cases shown in Fig. 7 demonstrate that in the downflowing case, the ion ratio depends very much on the upper boundary condition which is not known. We have made the simplifying assumption that the plasma is in equilibrium at the temperature where it starts to downflow. This does not at all have to be the case. The plasma could have been out of equilibrium in the upflowing process, and since ionizing and recombining plasmas behave differently, could depart from equilibrium even further.

The calculations presented in this paper demonstrate that temperature and density dependence as well as non-equilibrium effects must be carefully evaluated for each line ratio used in the diagnostic.

This work was supported by NASA contract NAS8-39073, and NASA grant NAG5-7055. We thank Randall Smith for the pre-release use of the APEC code, and the anonymous referee for valuable suggestions.

### REFERENCES

- Allen, C. W., 1976, *Astrophysical Quantities*, (London: Athlone Press).
- Bhatia, A.K. & Mason, H.E., 1980, *MNRAS*, 190, 925.
- Dankwort, W., and Treffitz, E., 1978, *A&A*, 65, 93.
- Edgar, R. J., and Chevalier, R. A. 1986, *ApJ*, 310, L27.
- Esser, R., Edgar, R. J., and Brickhouse, N. S. 1998, *ApJ*, 498, 448.
- Gaetz, T. J., Edgar, R. J., and Chevalier, R. A. 1988, *ApJ*, 329, 927.
- Hansteen, V.H., Leer, E., & Holzer, T.E., 1997, *ApJ*, 482, 498.
- Jordan, C., Doschek, G. A., Drake, J. J., Galvin, A., and Raymond, J. C. 1998, in *Cool Stars, Stellar Systems and the Sun*, eds. R. A. Donahue and J. A. Bookbinder. ASP conference series 154, 91.
- Landi, E., Landini, M., Dere, K. P., Young, P. R., & Mason, H. E., 1999, *A&AS*, 135, 339.
- Martin, W. C., Sugar, J., Musgrove, A., & Dalton, G. R., 1995 *NIST Database for Atomic Spectroscopy*, Version 1.0, NIST Standard Reference Database 61.
- Raymond, J. C., and Smith, B. W. 1977, *ApJS*, 35, 419.
- Sheeley, N. R. 1996, *ApJ*, 469, 423.
- Smith, R. K. & Brickhouse, N. S., 2000, *RevMexAA (Serie de Conferencias)*, 9, 134.
- Widing, K. G., Feldman, U., and Bhatia, A. K. 1986, *ApJ*, 308, 982.
- Widing, K. G., and Feldman, U., 1989, *ApJ*, 344, 1046.
- Widing, K. G., and Feldman, U., 1992, *ApJ*, 392, 715.
- Young, P. R. & Mason, H. E. 1997, *Sol. Phys.* 175, 523.
- Zhang, H. L., Graziani, M., and Pradhan, A. K., 1994, *A&A*, 283, 319.